HHS Public Access

Author manuscript

Sci Transl Med. Author manuscript; available in PMC 2016 July 14.

Published in final edited form as:

Sci Transl Med. 2016 June 15; 8(343): 343ra83. doi:10.1126/scitranslmed.aad5904.

Tissue-Engineered Autologous Grafts for Facial Bone Reconstruction

Sarindr Bhumiratana[1], **Jonathan C. Bernhard**[1], **David M. Alfi**[2], **Keith Yeager**[1], **Ryan E. Eton**[1], **Jonathan Bova**[3], **Forum Shah**[4], **Jeffrey M. Gimble**[4,5], **Mandi J. Lopez**[3], **Sidney B. Eisig**[1], and **Gordana Vunjak-Novakovic**[1,*]

[1]Department of Biomedical Engineering, Columbia University, 500 W 120th St., New York, NY 10027, USA

[2]Division of Oral and Maxillofacial Surgery, Columbia University College of Dental Medicine, 630 W 168th St., New York, NY 10032, USA

[3]School of Veterinary Medicine, Louisiana State University, Skip Bertman Dr., Baton Rouge, LA 70803, USA

[4]LaCell LLC, 1441 Canal St, New Orleans, LA 70112, USA

[5]Center for Stem Cell Research & Regenerative Medicine, Tulane University School of Medicine, 1324 Tulane Ave., SL-99, New Orleans, LA 70112, USA

Abstract

Facial deformities require precise reconstruction of the appearance and function of the original tissue. The current standard of care—the use of bone harvested from another region in the body—has major limitations, including pain and comorbidities associated with surgery. We have engineered one of the most geometrically complex facial bones by using autologous stromal/stem cells, without bone morphogenic proteins, using native bovine bone matrix and a perfusion bioreactor for the growth and transport of living grafts. The ramus-condyle unit (RCU), the most eminent load-bearing bone in the skull, was reconstructed using an image-guided personalized approach in skeletally mature Yucatan minipigs (human-scale preclinical model). We used clinically approved decellularized bovine trabecular bone as a scaffolding material, and crafted it into an anatomically correct shape using image-guided micromilling, to fit the defect. Autologous adipose-derived stromal/stem cells were seeded into the scaffold and cultured in perfusion for 3 weeks in a specialized bioreactor to form immature bone tissue. Six months after implantation, the

*Corresponding author: gv2131@columbia.edu (G.V.-N.).

Competing interests: The technology described in this paper is now being commercialized through a Columbia University spin-out, epiBone, co-founded by S.B., S.B.E. and G.V.N. J.M.G. is a co-owner, co-founder and Chief Scientific Officer of LaCell LLC, a for-profit company focusing on stromal/stem cell technology and clinical translation.

Author Contributions: S.B., S.B.E. and G.V.-N. designed experiments and developed the animal model. S.B. and G.V.N. wrote the manuscript. S.B., K.Y. and R.E.E were responsible for bioreactor design and fabrication. F.S. and J.M.G. isolated and characterized ASCs. S.B., J.C.B., and R.E.E. were responsible for tissue engineered bone graft manufacture, studies of the osteogenic differentiation, mechanical testing, histology, immunohistochemistry, CT, and μCT analysis. J.C.B. performed real-time PCR analysis and blinded image quantitation. R.E.E. performed DNA quantitation. D.M.A., M.J.L., and S.B.E performed animal surgery. J.B. and M.J.L. harvested adipose tissue and oversaw animal care.

Data and materials availability: All materials are available from commercial sources, or can be derived using methods described in this study. All relevant data are reported in the manuscript and the supplementary information.

engineered grafts maintained their anatomical structure, integrated with native tissues, and generated greater volume of new bone and greater vascular infiltration than either non-seeded anatomical scaffolds or untreated defects. This translational study demonstrates feasibility of facial bone reconstruction using autologous, anatomically shaped, living grafts formed *in vitro*, and presents a platform for personalized bone tissue engineering.

INTRODUCTION

Bone defects in the head and face due to congenital abnormalities, trauma or cancer surgery are associated with major functional, sociological, and psychological problems. Defects in the complex structures of the head and face are difficult to restore with aesthetic and functional accuracy. Bone autografts are the gold standard for craniofacial reconstruction, owing to their osteoinductive, osteoconductive, and immunocompatible properties (1, 2). However, autografts are limited in volume, associated with donor site morbidity, and are difficult to carve into precise anatomical shapes. Ideally, the craniofacial bones should be reconstructed to the original anatomy and using the patient's own cells.

Stem cell and tissue engineering approaches have made major strides towards growing biological substitutes that mimic the properties of native tissues. Clinically available bone grafts, either biological or synthetic, fall short of providing the fidelity of bone autografts, necessitating the development of new treatment modalities. Bone tissues grown from culture-expanded stem/progenitor cells isolated from bone marrow or adipose tissue aspirates, are now at the forefront of regenerative medicine (3–5). Enhanced bone regeneration by transplantation of various types of stem cells has been demonstrated in small animal models (6, 7). Other meritorious studies developed clinically sized anatomical scaffolds for bone reconstruction by growth factor delivery (8). Early on, imaging data were used in a single patient to create a titanium mesh that was filled with bone mineral, bone morphogenetic protein, and the patient's bone marrow; left for 7 months under a dorsal muscle to vascularize; and used to fit a mandible defect (9). Scaffolds with stem cells and growth factors were studied in large animal models, with growth factors alone or in combination with cells generally giving better outcomes (10–13).

However, translational studies in large animals of autologous bone engineered *in vitro* to precisely match the desired anatomy have not been conducted. The complexities associated with growing clinically sized, living bone grafts have been recognized (14, 15). We previously developed an anatomically correct scaffold-bioreactor system for bone tissue engineering using osteogenically differentiated mesenchymal stem cells (16). Additive manufacturing of tissue constructs has also been implemented in the repair of long bones (17). Our method is distinctly different as it engineers *in vitro* geometrically complex bones using autologous stem cells, anatomically shaped bone scaffolds, and a geometrically matched bioreactor chamber.

In this study, we move engineered bone tissues closer to humans by creating personalized scaffolds to heal critical-sized, load-bearing maxillofacial bone defects in skeletally mature large animals, the Yucatan minipig. The investigational approach was designed to provide clinical adequacy for repairing the RCU. We used decellularized bovine trabecular bone as a

scaffolding material, because it is a clinically approved for bone grafting (Cancello-Pure and CopiOs bone wedges), and crafted it into an anatomically correct shape to perfectly fit the defect by using image-guided micromilling. Autologous adipose-derived stromal/stem cells (ASCs) were the cells of choice due to their high availability and easy harvest when compared to bone marrow-derived cells (MSCs), along with osteogenic capacity (5, 18). The term “autologous” in this study refers to the use of cellular material prepared from a fat aspirate of the recipient animal and seeded into a cell-free bone matrix.

In addition to demonstrating feasibility and efficacy of bone repair, we recapitulated the logistics of the envisioned clinical application, where the patient and the manufacturing site are at remote locations, requiring shipping of both adipose tissues for cell isolation and bone grafts for implantation. The perfusion bioreactor was designed to allow the growth and transport of bone grafts in a single step, while maintaining sterility and viability. Thus, from start to finish, the study demonstrated utility and translation of personalized tissue-engineered bone grafts for facial reconstruction.

RESULTS

Bioreactor design for engineering anatomically shaped living bone implants

Our overarching objective was to grow bone grafts with the precise anatomical structure to repair a large defect in the jaw, without using bone morphogenic proteins (BMPs) or other growth factors; instead, we used only native bone matrix to induce osteogenic differentiation of ASCs, through its composition, architecture, and mechanical properties (7, 19, 20). We reconstructed the most eminent weight-bearing facial bone – the condyle-ramus unit (RCU), in Yucatan minipigs because of similarities in the jaw anatomy, mechanics and bone remodeling to those in humans.

We obtained the bone matrix by removing all cellular material from the native trabecular bone of bovine distal femur, and then fabricated the bone matrix into an exact anatomic replica of the native tissue structure (Fig. 1A). To this end, we used computer-aided micromilling fabrication methods that were guided by three-dimensional (3D) reconstructions of computer tomography (CT) images of each pig’s jaw. Autologous porcine ASCs were then cultured for three weeks in anatomically shaped scaffolds customized to each animal, in perfusion bioreactors (movie S1).

In order to maintain cell viability within these complex anatomical scaffolds, we devised an advanced bioreactor system that provided environmental control and the exchange of nutrients, oxygen and metabolites. The anatomical scaffold was placed into the matching void between two elastomer blocks containing arrays of channels designed based on the transport analysis. The elastomer blocks and the fluid-routing manifolds were aligned and tightened by the polycarbonate case to create a water-tight seal (Fig. 1B). The perfusion system distributed culture medium throughout the ~12-ml volume construct by regulating the fluid flow path resistance. Fluid distribution into the channels was directed by a fluid-routing manifold, via a peristaltic pump, with one inlet and one outlet per bioreactor. Gas exchange occurred within the media reservoir, to maintain oxygen and pH. The medium flow velocity at any specific location within the cultured graft was controlled by the size of

the channels that directed the fluid into and out of the anatomical chamber (Fig. 1C). For each animal, the channel sizes (0.82 to 2.41 mm) and channel locations were determined using computational flow simulation. The interstitial flow velocity of culture medium was maintained within the cultured grafts between 400 and 1000 μm/s (Fig. 1C) based on a previously determined optimum flow rate that did not limit oxygen transport to the cells (21).

Osteogenic differentiation of adipose stem cells and deposition of bone matrix

After three weeks of osteogenic differentiation in 2D culture, ASCs from subcutaneous porcine adipose tissue exhibited bone cell properties, including the deposition of alkaline phosphatase (ALP) and mineralized matrix (Fig. 2A,B). After 3 weeks of osteogenic culture in the 3D scaffolds, the cellularity of the grafts increased 7.5-fold relative to day 3 (Fig. 2C). Differentiated ASCs in the engineered bone grafts at week 3 expressed osteoblastic transcription factors, such as core-binding factor α1 (*Cbfa1*, also known as *Runx2*) and *Osterix*; osteogenic matrix proteins alkaline phosphatase (*Alp*), collagen type I (*Col1a1*), bone sialoprotein (*Bsp*), and osteonectin (*ON*); and osteogenic-related growth factors such as bone morphogenetic protein-2 (*Bmp2*) and transforming growth factor β2 (*Tgfb2*), normalized to internal *Gapdh* control and compared with day 3 (Fig. 2D). The ASCs attached to the bone scaffold surfaces, proliferated over 3 weeks of cultivation and filled the pore spaces (Fig. 2E). The cells and the new osteogenic extracellular matrix–rich in collagen type I and BSP were present throughout the graft interiors (Fig. 2E).

During graft transport to the site of implantation, the perfusion was discontinued for up to 10 hours. Finite element analysis of O_2 transport and consumption within 3D engineered bone grafts demonstrated that the minimal O_2 concentration at 10 hours was ≥0.14 mol/m^3 (movie S2), a value well above the depletion rate for cell survival. To test for the effects of reduced oxygen supply on cell viability, we conducted experiments with native osteochondral explants of a comparable thickness and showed that the cell viability did not change over a longer period of time (96 hours). The average percentage of live cells (± SD), determined by a live-dead assay, was 85 ± 12 for the freshly sectioned samples and 83 ± 6 after 96 hours of culture without medium perfusion. Consistently, the graft cellularity post-transport was not significantly different from the pre transportation values (Fig. 2C).

Pig RCU reconstruction model and bone regeneration

Fourteen skeletally mature Yucatan minipigs (>2 years old) were chosen as study subjects. The left RCU was excised (3-cm wide along the dorsal plane by 6-cm long along the transverse plane), with the right RCU left intact. The defects were fitted with a tissue-engineered bone graft or with a cell-free bone scaffold, or left untreated (condylectomy, to control for spontaneous regeneration). The animals were not immobilized, to maintain native loading environment. There were no complications throughout the 6-month study. Animals receiving acellular scaffolds and tissue-engineered bone were sacrificed at 3 months (n=2 each) or at 6 months (n=4 each). Condylectomy subjects were sacrificed at 6 months (n=2). The left temporomandibular joint (TMJ) capsule was excised with the base of the ramus and temporal bone intact. Engineered grafts had the exact anatomical shape of the native RCU extracted at the time of surgery (fig. S1).

Bone regeneration and condyle height—CT images of the porcine skulls were acquired immediately after surgery, and at 6 weeks, 3 months, and 6 months post-implantation (Fig. 3A, fig. S2). The bone volume (Fig. 3B) and the bone volume fraction (Fig. 3C) in the tissue engineered bone groups were significantly higher than in the acellular scaffold and condylectomy groups, at all time points. The greater amount of bone formed in the engineered grafts resulted in a more complete regeneration of the original joint anatomy, as indicated by the final heights of the new condyles (Fig. 3D). The extracted RCU unit was approximately 60% of the original height in all groups. After condylectomy, the condyle height reached approximately 80% of the structure height. Because the geometry and anatomical features of bone grafts matched the native RCU, the condyle height after implantation was equivalent to the physiologic height. Although the condyle height in the acellular scaffold group decreased over time, the condyle height in the engineered bone graft was maintained throughout the study (Fig. 3D).

Ramus regeneration—Regeneration of the ramus bone was initiated from the native bone and progressed towards the grafting region (Fig. 4A, fig. S2). Time lapse of CT images of the individual subjects revealed infiltration from the native bone at the rostral end and ossification at the caudal end of the ramus (Fig. 4A, fig. S2). Condylectomy resulted in incomplete ramus regeneration, with a large hollow area within the ramus observed by CT at 6 months following surgery (fig. S2). Histological analysis of the condylectomy control group revealed that the region lacking mineralized matrix was filled with soft fibrous tissue (Fig. 4B, fig. S3). The native and new bone could be distinguished by the presence of osteocytes that could only be observed in the newly formed bone.

In contrast to large amounts of acellular scaffold resorption as early as 3 months post-implantation (fig. S4), tissue-engineered bone grafts were gradually and orderly replaced by new bone, resulting in regeneration of the original tissues (fig. S5). Portions of both the implanted acellular scaffold and engineered bone were still present at 6 months following implantation (Fig. 4B, S3–5, S7–9), indicative of ongoing remodeling, with remarkable differences in the composition, structure, and bone formation between the two groups.

Condyle regeneration—Regeneration of the condyle could be seen in all groups at 6 months post-surgery (Fig. 4C, fig. S6). Longitudinal CT images of the individual subjects over 6 months revealed the patterns of condyle formation and ramus regeneration (fig. S6). In the condylectomy group, ossification occurred in the condyle region and grew in size over time, forming a condyle structure supported by a narrow ramus at the rostral and caudal ends (Fig. 4C). At 6 months, the condylar cartilage had not yet regenerated, resulting in underdeveloped condylar surfaces (Fig. 4D, fig. S7).

Acellular scaffold implantation resulted in new tissue at the articular surfaces of the graft material. By 3 months, the new bone formed at the articular region with only minimal formation of the condylar cartilage (Fig. 4, C and D; figs. S6 and S8). By 6 months, the ossification progressed and the articular cartilage formed at the condyle surfaces (Fig. 4D, figs. S6 and S8). Only small amounts of the original scaffold material were present within the newly formed condyle. By contrast, reconstruction with tissue-engineered bone resulted in the most complete condyle regeneration (Fig. 4, C and D; figs. S6 and S9). New bone

regenerated at the rostral side, and from the caudal end into the tissue engineered bone graft. Sites of endochondral ossification could be observed at the condylar surfaces, within the implanted tissue-engineered bone grafts (Fig. 4, fig. S10). After 6 months, the engineered bone graft was mostly replaced by the newly regenerated condyle containing a continuous layer of condylar cartilage (Fig. 4D; figs. S6, S9). The presence of portions of the implanted tissue engineered bone indicated continued regeneration and remodeling.

Graft-host integration

The structural integration of the implanted graft with native bone was investigated using high-resolution μCT and histological analysis. Paired histological (Movat's pentachrome) and μCT image analysis distinguished the implanted scaffold material (both acellular and cell-laden) from the native bone (Fig. 5A). Among the three experimental groups, the tissue-engineered grafts most strongly enhanced the graft-host bone integration. 3D reconstruction of engineered graft-host interface displayed the progression of structural integration between the new bone and the host bone at 3 months. Integration was confirmed by histology showing new bone penetrating into the graft (Fig. 5A). Higher-magnification histology revealed the proximity of the new bone and the resorbing scaffold, as well as the presence of osteoclastic processes involved in the remodeling and replacement of the graft material with the new bone. By 6 months, a large portion of the tissue-engineered bone graft was replaced by new bone (Fig. 4, B and D; Fig. 5A). In contrast, the implanted acellular scaffolds resulted in disconnected mineral structures with soft fibrous tissue formed between the host and the graft.

The mechanical integrity of regenerated bone was analyzed by 3-point bending (fig. S11) to determine structural stability of regenerating bone. The peak and equilibrium flexural moduli of the whole ramus were significantly higher for the tissue engineered bone group than the acellular scaffold group at both 3 and 6 month time points, but were still twofold lower than the corresponding values in native bone (Fig. 5, B and C). However, the peak force during bending the ramus after engineered bone implantation was similar to that of the native bone, indicating that the whole ramus tissue can withstand the same amount of flexural load as the native bone (Fig. 5C).

The mechanism of graft-host integration was investigated by evaluating the amounts and distributions of type I collagen and BSP. Preosteoblastic cells secreted rich extracellular matrix that underwent mineralization to form new bone containing osteocytes in the ramus region (Fig. 6). The new bone matrix was rich in type I collagen and BSP and ossified (Fig. 6). The cellularized region of this bone-like matrix was present pre-implantation (Fig. 2C) and maintained throughout the implantation study, suggesting that the osteogenically induced ASCs facilitated new bone formation and enhanced graft-host bone integration.

Scaffold structure, graft resorption, and vascular infiltration

Quantitative analysis of tissue microstructure was used to investigate the effects of stem cell incorporation on graft structure, resorption, and vascular infiltration. Large portions of the original graft material were still present 3 months following implantation (Fig. 7A), with the largest amount of the original scaffold material present in the tissue-engineered bone graft,

as determined by quantitative image analysis (Fig. 7 A,B) presumably due to lower rate of resorption (Fig. 7C). In contrast, the acellular scaffold underwent massive resorption *in vivo* with small dense macrophage-like cells infiltrating the grafts and amorphous areas consistent with tissue necrosis (Fig. 7A).

Notably, the tissue-engineered grafts vascularized, and the newly formed vasculature was continuous with the host circulation, as evidenced by the presence of blood cells inside lumen structures in Movat's pentachrome stains (Fig. 7A). Staining with H&E showed the formation of new vasculature, and the Prussian Blue stain confirmed the presence of hemoglobin (iron) in the cells found within the new blood vessels (Fig. 7D). The endothelial lining of the new blood vessels was confirmed by CD31 staining. Vasculature was also present in the acellular scaffold implantation, but to a markedly lower extent than in the tissue-engineered bone grafts (Fig. 7A,E). Interestingly, the vascularization was detected throughout the tissue engineered bone grafts (Fig. 4, B and D; fig S9), indicating that the formation of new bone and vascular perfusion occurred in parallel.

DISCUSSION

We developed a translational approach for growing anatomically correct bone grafts from autologous adipose-derived stem cells, and demonstrated its utility for reconstruction of the entire facial bone in a skeletally mature large animal. Cells were infused into an anatomically shaped decellularized bone scaffold and cultured in a matching bioreactor chamber with interstitial flow of culture medium, to engineer customized bone grafts. For each animal, the scaffold and the bioreactor were designed by image-guided fabrication. Over 6 months following implantation, the engineered grafts re-established the original RCU, integrated with the host bone, and formed bone-like tissue that was extensively vascularized, in contrast to both groups of control animals. This study is, to the best of our knowledge, the first to show tissue-engineered reconstruction of large, anatomically precise load-bearing craniofacial defect.

Previously, the utility of osteogenic stem cells has been studied in small animal models for craniofacial bone reconstruction (7, 8), and in sheep for regeneration of long bones by using MSCs seeded into scaffolds containing BMP-2 protein (10). We investigated regeneration of flat bones in the skull that involves intramembranous ossification preceded by callus formation (41, 42). Our system did not require addition of BMP-2, as the scaffold alone had strong osteogenic properties. For clinical impact, we created anatomically precise complex bone grafts using decellularized bone scaffolds and autologous MSCs, and demonstrated their utility for reconstructing load-bearing maxillofacial bone defects in a large animal model.

RCU, the most eminent load-bearing joint of the skull, served as a rigorous model for assessing tissue-engineered bone incorporation in skeletally mature minipigs. To mimic the envisioned logistics of the commercial process, the grafts were grown and implanted at two locations that were more than 1200 miles apart. For each animal, the CT images and adipose tissues were shipped to the processing laboratory. Cell preparation and assurance of quality followed good manufacturing guidelines (22–24), so that the process can be readily adapted

to the regulatory requirements. The bioreactor provided graft cultivation and transport to the implantation site in a closed system and with the preservation of cell viability. Grafts were implantated by an expert maxillofacial surgeon by following standard clinical protocols, and using standard plates and screws for fixation.

The study had two controls: condylectomy, to account for any spontaneous healing, and biomaterial scaffold, to account for the role of cells in inducing tissue regeneration. As in previous studies in large animals (37, 38), condylectomy resulted in minimal bone regeneration. The implanted acellular scaffolds resulted in formation of fibrous tissue, apparently due to insufficient capacity for replacing the degrading scaffold by new bone tissue. Only the tissue-engineered bone grafts enhanced condyle regeneration to the original height at both 3 and 6 months, while maintaining mechanical integrity of the ramus. The condylar cartilage formed at the articular surface and the subchondral bone replaced the implanted bone graft, resulting in high fidelity of the regenerated condylar surface. Unlike acellular scaffolds, the scaffold material in tissue-engineered bone grafts was degraded slowly and replaced by new bone. Fast resorption of acellular scaffolds caused inflammatory responses and soft tissue infiltration that persisted through 6 months of implantation. These properties of acellular scaffolds have led to granulation and fibrosis at the graft-host interface, precluding graft incorporation (35). In contrast, engineered bone grafts enhanced bone ingrowth, provided mechanical stability for mastication, and accelerated graft turnover and new bone formation. These properties are important for clinical translation as the success in clinical bone grafting depends on graft resorption, bone incorporation, and mechanical stability. Clearly, graft resorption needs to be balanced with the deposition and remodeling of the new bone for adequate craniofacial reconstruction (36). We believe that slower bulk resorption and the presence of osteoclasts in tissue-engineered bone supported favorable remodeling into native-like bone.

Similar to previous studies that employed perfusion bioreactors for bone tissue engineering (16, 21, 25), the grafts contained large numbers of cells ($\geq 6\times10^8$ cells) expressing osteogenic markers *CBFA1* and *Osterix* (26, 27) with dense bone ECM filling the scaffold pores. The differentiating ASCs expressed high levels of bone-related genes and proteins, such as alkaline phosphatase, collagen I, bone sialoprotein and osteonectin. Of note, BMP-2 [commonly added to support bone culture and repair (30)] and transforming growth factor-β2 (28, 29), were also highly expressed in engineered grafts at 3 and 6 months following implantation. Consistent with previously shown immunoprotective and anti-inflammatory properties of MSCs, including ASCs (31–34), tissue-engineered bone grafts did not express pro-inflammatory genes.

Vascularization of implanted tissues has been a major challenge, as inadequate nutrient transport leads to necrosis (43). Culture-expanded stromal/stem cells have been shown to promote endothelial migration and induced angiogenesis both *in vitro* and *in vivo* (44–46). In our study, vascularization was associated with the formation of new bone in the regenerating RCU, and detected deep inside the graft, as in autologous trabecular bone implants, where bone was vascularized rapidly through the marrow spaces (2). These regenerative features were not seen in acellular scaffolds, suggesting that the autologous ASCs exhibited osteoconductive and osteoinductive properties as reported for autologous

trabecular bone implants (2). Nevertheless, the comparison between engineered bone grafts and tissue autografts needs a more detailed evaluation of the integrative repair at the graft-host interface, and vascular perfusion.

We demonstrated that bone grafts engineered to the exact anatomical shape using decellularized bone scaffolds and autologous ASCs regenerated the entire RCU in a pig model. However, our study also has limitations. We did not determine if enhanced bone formation was a direct effect of implanted cells, or a result of secondary factors, such as immune modulation, pro-angiogenic signaling, and/or release of chemotactic or homing signals. Cell lineage tracking will be required to discern possible mechanisms. It will also be of interest to compare ASCs to alternative sources of autogenous cell populations, and to determine effects of cell concentration and the duration of bioreactor culture on integrative repair. Lastly, translation of tissue-engineered grafts into clinical use will require characterization of ASCs from diverse donor populations to ensure quality control and safety.

Materials and Methods

Study design

The objective of our study was to engineer anatomically correct living craniofacial bones by using autologous stromal/stem cells without bone morphogenic proteins, using native bone matrix, a perfusion bioreactor, and image-guided fabrication methods. Our pre-specified hypothesis was that the immature bone formed *in vitro* will serve as a template for bone development and remodeling and its functional integration with adjacent host tissues. The research was conducted using skeletally mature Yucatan minipigs [21 to 32 months old; 48 to 73 kg (60.0 ± 7.9 kg)]. Sample size was determined using power analysis (β=0.1 and α=0.05) with μ_A and μ_B of 0.4 and 0.6, respectively, and standard deviation of 0.1 based on estimated bone volume fraction. The resulting sample size was 6.

Anatomically correct engineered bone grafts were investigated for their capacity to regenerate the entire ramus-condyle unit during a 6-month period of implantation in Yucatan minipig. Two control groups were studied: condylectomy (to assess any spontaneous regeneration of the bone) and acellular, anatomically shaped scaffolds (to assess the role of exogenous cells in tissue regeneration). Tissue outcomes were evaluated by using CT and μCT imaging, gene expression, protein contents, histology, immunostains and biomechanical testing. Selection of animals for the main experimental group and the two control groups was randomized. In the main experimental group, the cells were autologous and therefore derived from each animal. Also, the scaffold and bioreactor chamber were specifically made for each animal to fit the defect geometry, by image-guided fabrication. The acellular scaffold group also required the image-guided preparation of a specific scaffold for each animal. The implantations could not be blinded because of the different appearance of the engineered bone (tissue-like) and acellular scaffold (biomaterial-like). Nevertheless, all analytical assessments were blinded to the maximum practical extent, and most of them were done by an independent expert (such as μCT, CT, histology, mechanical testing) to eliminate any bias.

Stromal/stem cell preparation

Subcutaneous fat (approximately 20 g) was harvested from the dorsal lumbar region of each animal ($n = 7$) at the same time as the initial CT procedure and the adipose-derived stem cells were isolated as previously described (23). The flasks containing P0 ASCs were completely filled with culture medium and shipped on ice to Columbia University for processing. The pASCs were expanded in DMEM, 10% FBS, 1% pen/strep (P/S), and 0.1 ng/ml fibroblast growth factor, and passaged by trypsinization up to passage 3 (P3).

Scaffold fabrication

The scaffolds were made from native bovine bone, after removing all cellular material to leave behind the extracellular matrix with largely preserved composition, architecture and mechanical properties. The decellularization method has been demonstrated to remove all cellular material from the bone (47). Large cancellous bone blocks were created from the distal aspect of adult bovine femurs (>2 year old) after removing the epiphysis, articular surface, and periosteum with an electrical band saw. The blocks were lathed into cylinder blocks 4.5-cm in diameter × 12 cm long. To fabricate an anatomical TMJ ramus-condyle cancellous bone block, G-Code was generated from the Initial Graphics Exchange Specifications (.iges) files of the CT images for each pig, using MasterCAM software. Using a 4-axis computer numerical control milling machine (LittleMachineShop), the cylindrical bone blocks were milled into the custom geometry of the RCU for each pig. The anatomical scaffolds were decellularized by using a modification of a known protocol (16), and is described in Supplementary methods.

Perfusion bioreactor design and operation

The perfusion bioreactor used in this study was developed starting from our previous bioreactor system that was used to generate anatomical pieces of tissue-engineered bone with high cell density (16), and is described in Supplementary methods.

Cultivation of bone grafts

The anatomically shaped scaffolds were seeded and cultured using perfusion bioreactors with anatomical chambers fabricated to exactly match the geometry of each scaffold, as described above. For scaffold seeding, the scaffold volumes were determined by the SolidWorks software, and were in the range of 11–15 cm^3. A suspension of P3 pASCs (12 mL, 10^7 cells/cm^3 in expansion media) was injected into the culture chamber throughout the anatomical scaffold. After allowing the cells to attach for 3 hours at 37°C in an incubator, while osteogenic media (low glucose DMEM supplemented with 10% FBS, 1% antibiotics, 10 mM sodium-β-glycerophosphate, 100 nM dexamethasone, and 50 mg/ml ascorbic acid-2-phosphate) were perfused through the scaffold for 3 days at 10% of the calculated optimal flow rate, to promote spatially uniform cell attachment throughout the scaffold volume.

For cultivation of bone grafts, the seeded scaffolds were perfused with osteogenic medium for 3 weeks at the set optimal flow rate, with medium changes twice per week. The 3-week cultivation period was selected based on the finding that ASCs highly express osteogenic markers after 3 weeks of in vitro differentiation (fig. S2). Four engineered constructs were generated for each animal: one for implantation and three for evaluation, after 3 days and 3

weeks of cultivation, and following transport from New York, NY, to Baton Rouge, LA, where the grafts were implanted. Transport of the bone grafts is described in Supplementary methods.

Animal implantation study

The animal implantation study was conducted at the Louisiana State University under an approved IACUC protocol. A total of fourteen skeletally mature Yucatan minipigs were divided into three groups: (i) condylectomy (n=2), (ii) acellular scaffold implantation (n=6), and (iii) autologous engineered bone implantation (n=6). Two surgeries were performed per day, over a period of two months. Two pigs per group receiving acellular scaffold or autologous tissue engineered bone graft were sacrificed at three months post implantation. The remaining animals were sacrificed at 6 months. CT imaging was performed immediately and after 6 weeks, 3 months, and 6 months after surgery. Endpoint analyses included mechanical testing, histological, and immunohistological evaluation and gene expression.

All pigs underwent clinical CT scan (GE Lightspeed 16; 120 kVp 625 μm resolution) 2–3 months prior to surgery. For each animal, the facial skull structures were reconstructed from CT images using the Mimics software. From the reconstructed 3D images, we selected the left TMJ ramus-condyle unit measuring 3-cm along the dorsal plane by 6-cm along the transverse plane as the region for defect creation and reconstruction. For all animals except the condylectomy controls, the 3D structure data were sent to the lab at Columbia University and the defect/grafting region was selected in Mimics software.

The animal implantation process and the selection of fixative method were chosen by an expert maxillofacial surgeon to closely mimic the current clinical procedure. The implantation procedure occurred after 12 hours of food withdrawal. The pigs were administered intramuscularly with ketamine (10 mg/kg, Vedco Inc), midazolam (0.2 mg/kg, Hospira, Inc), and dexmedetomidine (2 μg/kg, Pfizer Animal Health). Anesthesia was induced 15 minutes later with 5% isoflurane in 100% oxygen at 1.5 l/min flow via facial mask. The animals were intubated with a cuffed Murphy’s endotracheal tube (7–9 mm internal diameter) and anesthesia was maintained at a vaporizer setting of 1.5% isoflurane in a circular breathing system.

The pigs were then prepped and draped in a standard sterile fashion. We used a retromandibular approach with a 15 blade to make a 5-cm skin incision. We then used electrocautery to dissect through the subcutaneous and superficial cervical fascial layers. Blunt dissection was carried to the angle and inferior border of the mandible, where the periosteum was approached. The facial vessels were identified and ligated. The periosteum was incised with electrocautery and sub-periosteal dissection exposed the medial and lateral mandible from the antegonial notch to the head of the condyle. Pre-planned cuts were measured and marked and condylectomies were performed with a reciprocating saw under copious sterile saline irrigation. The RCU was then removed and the pig was either treated with no replacement (condylectomy) or replacement with an acellular scaffold or a tissue engineered bone graft. Two 8-hole miniplates with 1.7-mm bone screws (Stryker) were used

to provide rigid fixation of the implants. The wounds were closed with 3-0 polyglactin 910 sutures for subcutaneous tissues and 2-0 nylon sutures for skin.

CT and μCT Imaging

The animals were anesthetized and placed in ventral recumbancy on the GE LightSpeed 16 Slice CT scanner (GE Medical Systems). The scans (0.625 mm resolution, 120 kV) were conducted on all animals at 2 months pre-surgery, immediately, and at 6 weeks, 3 months, and 6 months following surgery. μCT imaging (50 μm resolution, 100 kV) of harvested RCUs was done using the GE Explore CT-120 (GE Medical Systems) at an external facility (Cornell University Imaging Facility), in a blinded fashion. Condyle height and bone volume were measured using the Mimics software (Materialise). Quantitation of bone volume and bone volume fraction was conducted by determining the amount of bone in the defect area based on the difference between the CT of pre- and post- surgery and the amount of bone removed.

μCT was performed by using a modified protocol (47), and the samples were scanned at 21-μm isotropic resolution. The bone volume was obtained from the application of a global thresholding technique so that only the mineralized tissue was detected. There was no difficulty in distinguishing the grafted material from the miniplates and screws used for fixation, which appeared in μCT as compact and geometrically defined structures. Spatial resolution of the full-voxel model was sufficient for evaluating the microarchitecture of the bone tissue.

Mechanical testing

A simple 3-point bending mechanical test was utilized to assess structural rigidity of the ramus (fig. S11). Samples were cut along dorsal plane into approximately 1-cm wide (ventral-dorsal) and 3-cm long (cranial-caudal). Two 1-cm sections were cut and tested for each animal sacrificed at 3-month and for condylectomy group; and one 1-cm section was cut and tested for other animals. Soft tissue was removed to expose the hard tissue structure. The samples were placed on two supports that were 25 mm apart. An actuator applied a load in the exact middle of the two supports onto the samples. Preload of 25 g was applied for 900 seconds prior to the test. The samples were subjected to a 300-μm displacement at a loading rate of 3 μm/s and then held in place for 1800 seconds. Force was measured throughout the period of loading. Peak force and equilibrium force were determined as the maximum force and the force at the end point of the testing. The flexural modulus (E) was calculated from the force measured and the geometry of the sample:

$$E=\frac{Fl^3}{48yI}$$

where F is force, l is the distance between two supports, y is the displacement, and I is the overall second moment of area which was calculated using a solid rectangular beam model:

$$I=\frac{wh^3}{12}$$

where w and h are width and height of the samples, respectively.

Statistical Analysis

Statistical analysis was conducted using Graphpad Prism software (GraphPad Software Inc). Statistical analysis of graft cellularity was carried out by one-way ANOVA nonparametric test and Tukey's comparison post-test to compare means. Statistical analysis of gene expression was carried out by the one-sample t test with hypothetical value of 1. Statistical analyses of the bone volume, bone volume fraction, condyle height, and mechanical properties were carried out by two-way ANOVA and Bonferroni post-hoc tests to compare the means. Data were calculated as the means ± SD. Statistical analyses of image quantitation was carried out by Student's t-test. $P < 0.05$ was considered significant. The box plots were constructed to represent median, first quartile, and third quartile, with error bars indicating maximum and minimum values; if outliers are present, they are shown as dots above or below. Histograms are mean mean ± 1SD. Dot plots are individual animals with lines to represent the mean ± 1SD.

Supplementary Material

Refer to Web version on PubMed Central for supplementary material.

Acknowledgments

We thank the staff at the Lousiana State University School of Veterinary Study for veterinary assistance.

Funding: We gratefully acknowledge funding support by NIH (grants DE016525 and EB002520), the New York Partnership Bioaccelerate Program (CU11- 1915), and Mikati Foundation (gift funding for research).

References and Notes

1. Giannoudis PV, Dinopoulos H, Tsiridis E. Bone substitutes: an update. Injury. Nov.2005 36(Suppl 3):S20. [PubMed: 16188545]
2. Yaszemski MJ, Payne RG, Hayes WC, Langer R, Mikos AG. Evolution of bone transplantation: molecular, cellular and tissue strategies to engineer human bone. Biomaterials. Jan.1996 17:175. [PubMed: 8624394]
3. Caplan AI. Review: mesenchymal stem cells: cell-based reconstructive therapy in orthopedics. Tissue engineering. Jul-Aug;2005 11:1198. [PubMed: 16144456]
4. Gimble J, Guilak F. Adipose-derived adult stem cells: isolation, characterization, and differentiation potential. Cytotherapy. 2003; 5:362. [PubMed: 14578098]
5. Pittenger MF, et al. Multilineage potential of adult human mesenchymal stem cells. Science. Apr 2.1999 284:143. [PubMed: 10102814]
6. Cowan CM, et al. Adipose-derived adult stromal cells heal critical-size mouse calvarial defects. Nature biotechnology. May.2004 22:560.
7. Meinel L, et al. Silk implants for the healing of critical size bone defects. Bone. Nov.2005 37:688. [PubMed: 16140599]
8. Hollister SJ, et al. Engineering craniofacial scaffolds. Orthodontics & craniofacial research. Aug. 2005 8:162. [PubMed: 16022718]

9. Warnke PH, et al. Growth and transplantation of a custom vascularised bone graft in a man. Lancet. Aug.2004 364:766. [PubMed: 15337402]
10. Reichert JC, et al. A tissue engineering solution for segmental defect regeneration in load-bearing long bones. Science translational medicine. Jul 4.2012 4:141ra93.
11. Yamada Y, Ito K, Nakamura S, Ueda M, Nagasaka T. Promising cell-based therapy for bone regeneration using stem cells from deciduous teeth, dental pulp, and bone marrow. Cell transplantation. 2011; 20:1003. [PubMed: 21054950]
12. Berner A, et al. Delayed minimally invasive injection of allogenic bone marrow stromal cell sheets regenerates large bone defects in an ovine preclinical animal model. Stem cells translational medicine. May.2015 4:503. [PubMed: 25834121]
13. Field JR, et al. The efficacy of allogeneic mesenchymal precursor cells for the repair of an ovine tibial segmental defect. Veterinary and comparative orthopaedics and traumatology: VCOT. 2011; 24:113. [PubMed: 21225086]
14. Bancroft GN, Sikavitsas VI, Mikos AG. Design of a flow perfusion bioreactor system for bone tissue-engineering applications. Tissue engineering. Jun.2003 9:549. [PubMed: 12857422]
15. Gaspar DA, Gomide V, Monteiro FJ. The role of perfusion bioreactors in bone tissue engineering. Biomatter. Oct-Dec;2012 2:167. [PubMed: 23507883]
16. Grayson WL, et al. Engineering anatomically shaped human bone grafts. Proceedings of the National Academy of Sciences of the United States of America. Feb 23.2010 107:3299. [PubMed: 19820164]
17. Costa PF, et al. Biofabrication of customized bone grafts by combination of additive manufacturing and bioreactor knowhow. Biofabrication. Sep.2014 6:035006. [PubMed: 24809431]
18. Gupta A, et al. Osteo-maturation of adipose-derived stem cells required the combined action of vitamin D3, beta-glycerophosphate, and ascorbic acid. Biochemical and biophysical research communications. Oct 12.2007 362:17. [PubMed: 17692823]
19. de Peppo GM, et al. Engineering bone tissue substitutes from human induced pluripotent stem cells. Proceedings of the National Academy of Sciences of the United States of America. May. 2013 110:8680. [PubMed: 23653480]
20. Marolt D, et al. Engineering bone tissue from human embryonic stem cells. Proceedings of the National Academy of Sciences of the United States of America. May.2012 109:8705. [PubMed: 22586099]
21. Grayson WL, et al. Optimizing the medium perfusion rate in bone tissue engineering bioreactors. Biotechnology and bioengineering. May.2011 108:1159. [PubMed: 21449028]
22. Estes BT, Diekman BO, Gimble JM, Guilak F. Isolation of adipose-derived stem cells and their induction to a chondrogenic phenotype. Nature protocols. Jul.2010 5:1294. [PubMed: 20595958]
23. Williams KJ, et al. Isolation and characterization of porcine adipose tissue-derived adult stem cells. Cells, tissues, organs. 2008; 188:251. [PubMed: 18349524]
24. Riis S, et al. Critical steps in the isolation and expansion of adipose-derived stem cells for translational therapy. Expert reviews in molecular medicine. 2015; 17:e11. [PubMed: 26052798]
25. Sikavitsas VI, Bancroft GN, Holtorf HL, Jansen JA, Mikos AG. Mineralized matrix deposition by marrow stromal osteoblasts in 3D perfusion culture increases with increasing fluid shear forces. Proceedings of the National Academy of Sciences of the United States of America. Dec 9.2003 100:14683. [PubMed: 14657343]
26. Cao Y, et al. Osterix, a transcription factor for osteoblast differentiation, mediates antitumor activity in murine osteosarcoma. Cancer research. Feb 15.2005 65:1124. [PubMed: 15734992]
27. Ducy P. Cbfa1: a molecular switch in osteoblast biology. Developmental dynamics: an official publication of the American Association of Anatomists. Dec.2000 219:461. [PubMed: 11084646]
28. Centrella M, Horowitz MC, Wozney JM, McCarthy TL. Transforming growth factor-beta gene family members and bone. Endocrine reviews. Feb.1994 15:27. [PubMed: 8156937]
29. Chen D, Zhao M, Harris SE, Mi Z. Signal transduction and biological functions of bone morphogenetic proteins. Frontiers in bioscience: a journal and virtual library. Jan 1.2004 9:349. [PubMed: 14766372]

30. McKay WF, Peckham SM, Badura JM. A comprehensive clinical review of recombinant human bone morphogenetic protein-2 (INFUSE Bone Graft). International orthopaedics. Dec.2007 31:729. [PubMed: 17639384]
31. Le Blanc K, Tammik C, Rosendahl K, Zetterberg E, Ringden O. HLA expression and immunologic properties of differentiated and undifferentiated mesenchymal stem cells. Experimental hematology. Oct.2003 31:890. [PubMed: 14550804]
32. McIntosh K, et al. The immunogenicity of human adipose-derived cells: temporal changes in vitro. Stem cells. May.2006 24:1246. [PubMed: 16410391]
33. Prockop DJ, Oh JY. Mesenchymal stem/stromal cells (MSCs): role as guardians of inflammation. Molecular therapy: the journal of the American Society of Gene Therapy. Jan.2012 20:14. [PubMed: 22008910]
34. van den Berk LC, et al. Mesenchymal stem cells respond to TNF but do not produce TNF. Journal of leukocyte biology. Feb.2010 87:283. [PubMed: 19897767]
35. Bauer TW, Muschler GF. Bone graft materials. An overview of the basic science. Clinical orthopaedics and related research. Feb.2000 10
36. Elsalanty ME, Genecov DG. Bone grafts in craniofacial surgery. Craniomaxillofacial trauma & reconstruction. Oct.2009 2:125. [PubMed: 22110806]
37. Miyamoto K, et al. Effect of unilateral condylectomy on the sheep temporomandibular joint. The British journal of oral & maxillofacial surgery. Oct.1999 37:401. [PubMed: 10577756]
38. Poswillo DE. The late effects of mandibular condylectomy. Oral surgery, oral medicine, and oral pathology. Apr.1972 33:500.
39. Boskey AL. Noncollagenous matrix proteins and their role in mineralization. Bone and mineral. May.1989 6:111. [PubMed: 2670018]
40. Colfen H. Biomineralization: A crystal-clear view. Nature materials. Dec.2010 9:960. [PubMed: 21102512]
41. Karp NS, McCarthy JG, Schreiber JS, Sissons HA, Thorne CH. Membranous bone lengthening: a serial histological study. Annals of plastic surgery. Jul.1992 29:2. [PubMed: 1497292]
42. Yang YQ, et al. The role of vascular endothelial growth factor in ossification. International journal of oral science. Jun.2012 4:64. [PubMed: 22722639]
43. Kaully T, Kaufman-Francis K, Lesman A, Levenberg S. Vascularization--the conduit to viable engineered tissues. Tissue engineering Part B, Reviews. Jun.2009 15:159. [PubMed: 19309238]
44. Traktuev DO, et al. A population of multipotent CD34-positive adipose stromal cells share pericyte and mesenchymal surface markers, reside in a periendothelial location, and stabilize endothelial networks. Circulation research. Jan 4.2008 102:77. [PubMed: 17967785]
45. Trkov S, Eng G, Di Liddo R, Parnigotto PP, Vunjak-Novakovic G. Micropatterned three-dimensional hydrogel system to study human endothelial-mesenchymal stem cell interactions. Journal of tissue engineering and regenerative medicine. Mar.2010 4:205. [PubMed: 19998330]
46. Wu Y, Chen L, Scott PG, Tredget EE. Mesenchymal stem cells enhance wound healing through differentiation and angiogenesis. Stem cells. Oct.2007 25:2648. [PubMed: 17615264]
47. Grayson WL, et al. Effects of initial seeding density and fluid perfusion rate on formation of tissue-engineered bone. Tissue engineering Part A. Nov.2008 14:1809. [PubMed: 18620487]

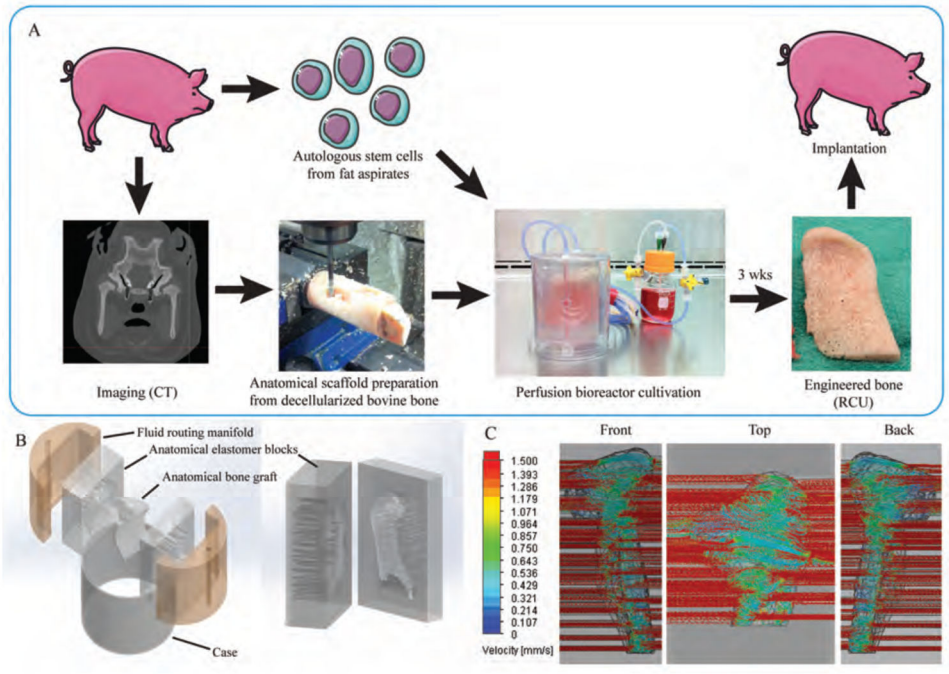

Figure 1. Fabrication of engineered bone grafts

(A) Personalized bone tissue engineering process. Autologous mesenchymal stem cells (from fat aspirates) and CT images were obtained for each animal subject. The anatomical scaffold was fabricated from the bovine stifle bone that had been processed to remove any cellular material while preserving the tissue matrix. The cells were seeded into the scaffold and cultured in the specially designed perfusion bioreactor. After 3 weeks, the engineered RCU was implanted back into the pig for 6 months. **(B)** The bioreactor culture chamber consisted of five components designed to provide tightly controlled perfusion through the anatomical scaffold: anatomical inner chamber with bone scaffold; two halves of the polydimethylsiloxane (PDMS) (elastomer) block with incorporated channels; two manifolds; and an outer casing. The PDMS block was designed as an impression of the anatomical RCU structure, and contained flow channels at both sides for the flow of culture medium in and out of the scaffold. The flow rate necessary for providing nutrient supply and hydrodynamic shear was defined by the design of parallel channels in the elastomer block (with the channel diameters and distribution dictated by the geometry of the graft) and the fluid routing manifold. The channel diameters and spacing were specifically designed by flow simulation software for each pig, to provide a desired interstitial flow velocity for a given shape and size of the anatomical RCU. **(C)** Flow simulation of the medium flow through the anatomically shaped scaffold reveals uniform flow velocity throughout the volume of the graft.

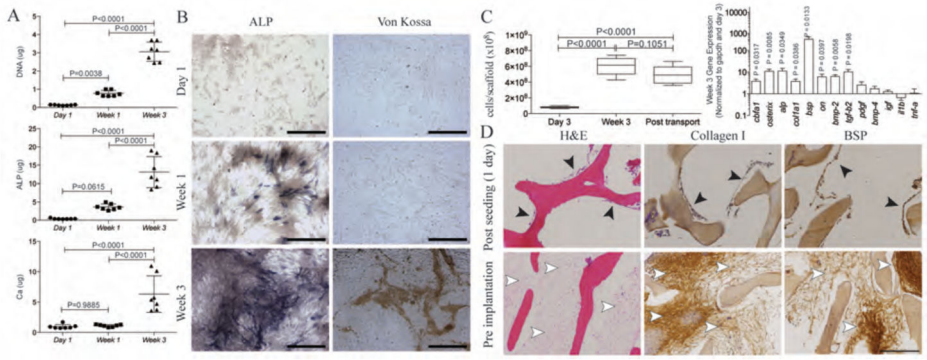

Figure 2. Properties of engineered bone grafts

(A) DNA, alkaline phosphatastase (ALP), and calcium (Ca) content over the course of 3-weeks of osteogenic induction. Significant increases in ALP and Ca deposition were observed. Data were quantified for each animal as a mean ± SD (n = 7 animals), using one-way ANOVA and Tukey's comparison post-test. **(B)** Alkaline phosphatase and von Kossa stains confirmed deposition of alkaline phosphatase protein and mineral during osteogenic induction. **(C)** DNA content quantifies the number of cells per scaffold at 3 days and 3 weeks after osteogenic induction in the scaffold-bioreactor system, as well as after transport (one additional day). Data are box plots ($n = 7$). P values determined by one-way ANOVA with Tukey's multiple comparison post-hoc test. (**D**) Gene expression after 3 weeks of osteogenic induction of cells in the scaffold. Data are the fold difference (mean ± SD) of gene expression normalized to the housekeeping gene (*Gapdh*) and then to the corresponding day 3 data ($n = 7$). P values determined by t-test with $H_0 = 1$. **(E)** H&E staining and immunohistochemistry (type I collagen, BSP) of engineered bone grafts after seeding (3 days) and before implantation (3 weeks). Cells attached to the scaffold (black arrowheads), proliferated, filled the pore spaces, and deposited bone proteins (white arrowheads). The decellularized trabecular scaffold (S) was maintained throughout the cultivation period. Scale bars: 250 μm.

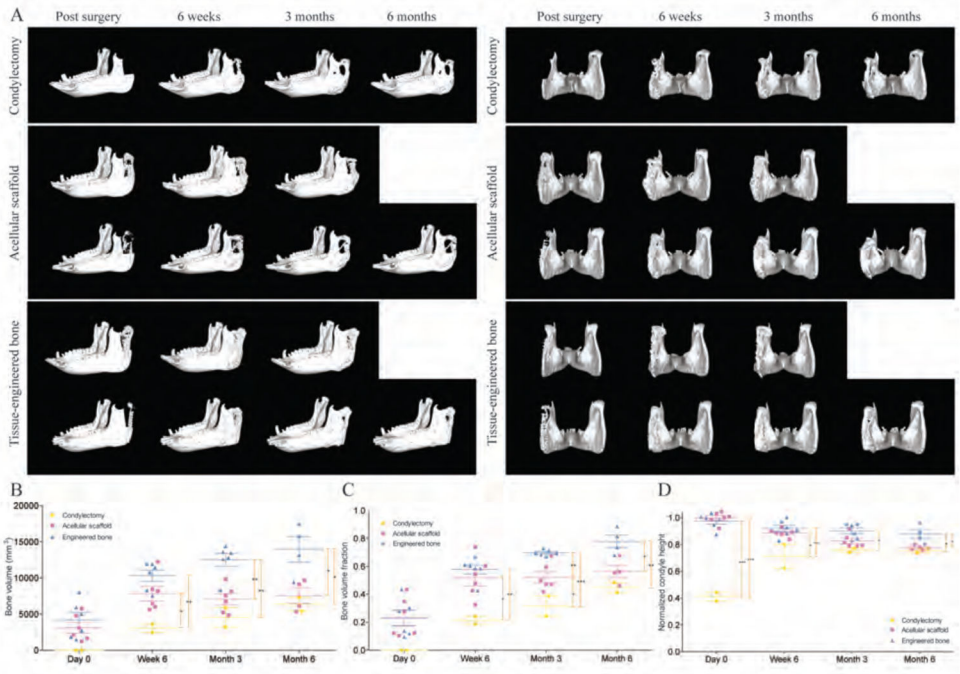

Figure 3. Progression of bone regeneration and reestablishment of condyle height

(A) Lateral (left) and caudal (right) 3D views of the mandible after surgery. Images were taken at timed intervals for condylectomy controls ($n = 1$), animals implanted with acellular scaffolds ($n = 2$), and animals implanted with tissue-engineered bone ($n = 2$). Additional images are in fig. S2. **(B** to **D)** Quantitative analysis of bone volume (B), bone volume fraction (C), and condyle height normalized to the original height (D). Data are individual animals with means ± SD ($n = 6$). ***p<0.001; **p<0.01; *p<0.05, two-way ANOVA and Bonferroni post-hoc tests.

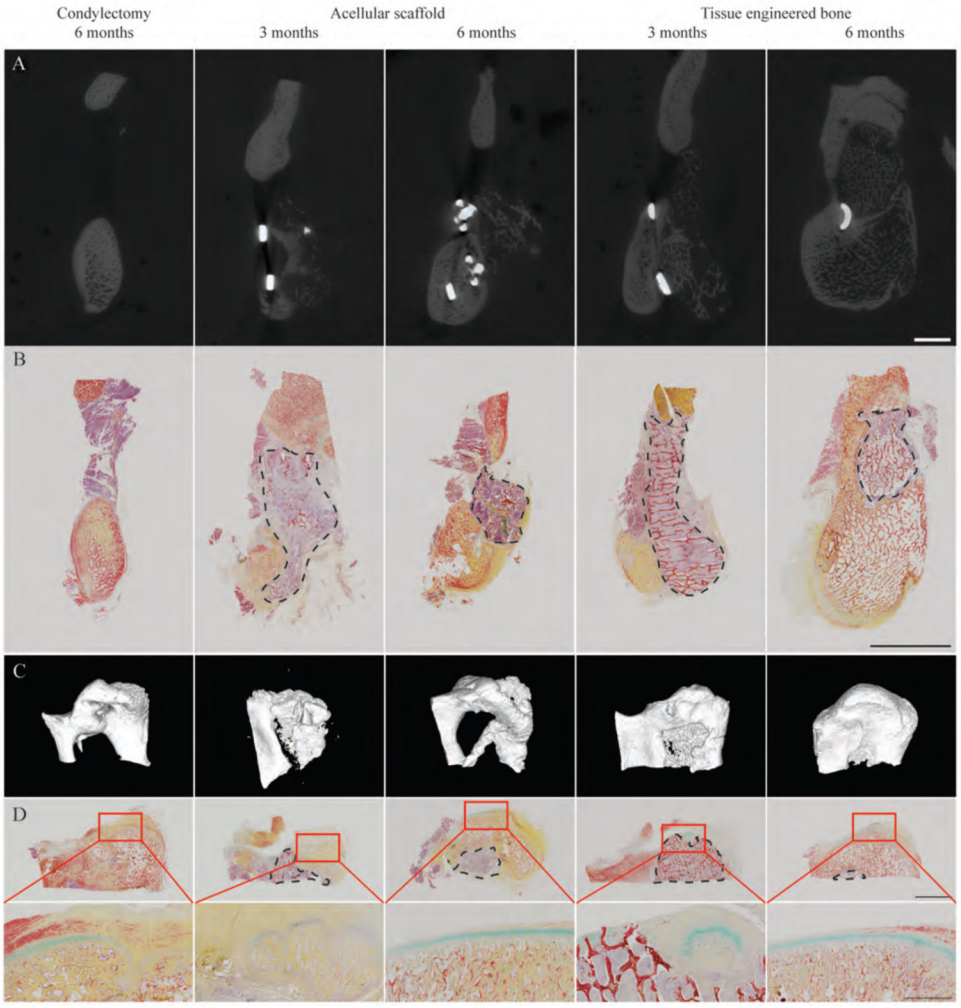

Figure 4. Morphology and structure of regenerated ramus-condyle unit (RCU)

(**A** and **B**) Ramus regeneration was assessed by μCT (A) and Movat's pentachrome staining for bone and soft tissues (B). Scale bars, 1 cm. (**C** and **D**) Condyle regeneration was assessed using μCT 3D reconstruction (C) and Movat's pentachrome staining (D) at low magnification (top, 1 cm scale) and high magnification (bottom, 2 mm scale) of the condylectomy site. The dashed circumferences indicate the remaining graft regions with the red trabecular structure representing the remaining scaffold material. Images are representative of $n = 2$ (condylectomy control), n = 4 (acellular scaffold), and n = 4 (tissue-engineered bone) animals.

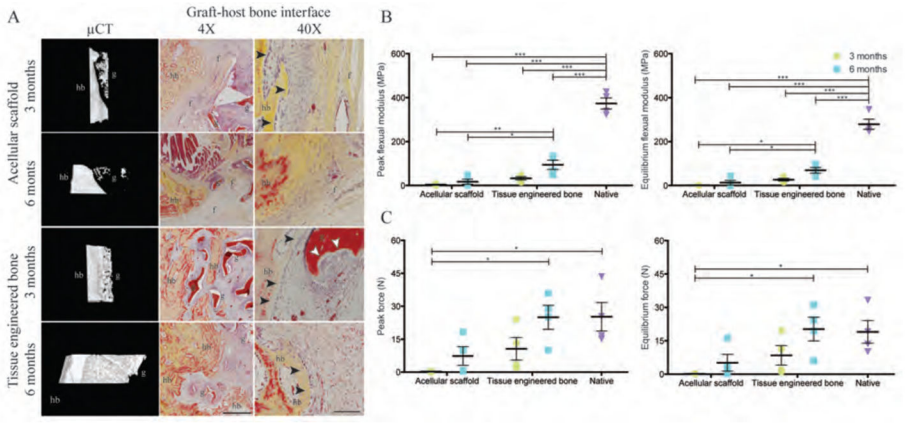

Figure 5. Graft-host bone integration

(A) μCT 3D reconstruction of the graft-host interface and Movat's pentachrome staining were used to assess integration of the implanted graft with the host bone. For acellular grafts, the mineralized host bone (hb) and the graft structures (g) were separated by soft fibrous tissue (f). In contrast, host bone (hb) extended into the tissue-engineered bone graft (g). In the proximity of the new bone, osteoclastic resorption (white arrowheads) was detected on the implanted scaffold with the lining of osteoblasts (black arrowheads), indicating active ossification. Scale bars: 1 mm (4×) and 100 μm (40×). (**B** and **C**) Three-point bending mechanical test for peak and equilibrium flexural moduli (B) and the peak and equilibrium forces (C). Data are means ± SD (n=4 from 2 animals for condylectomy; n=4 from 2 animals for 3 months data; n=8 from 4 animals for 6 month data). ***p<0.001; **p<0.01; *p<0.05, two-way ANOVA and Bonferroni post-hoc tests.

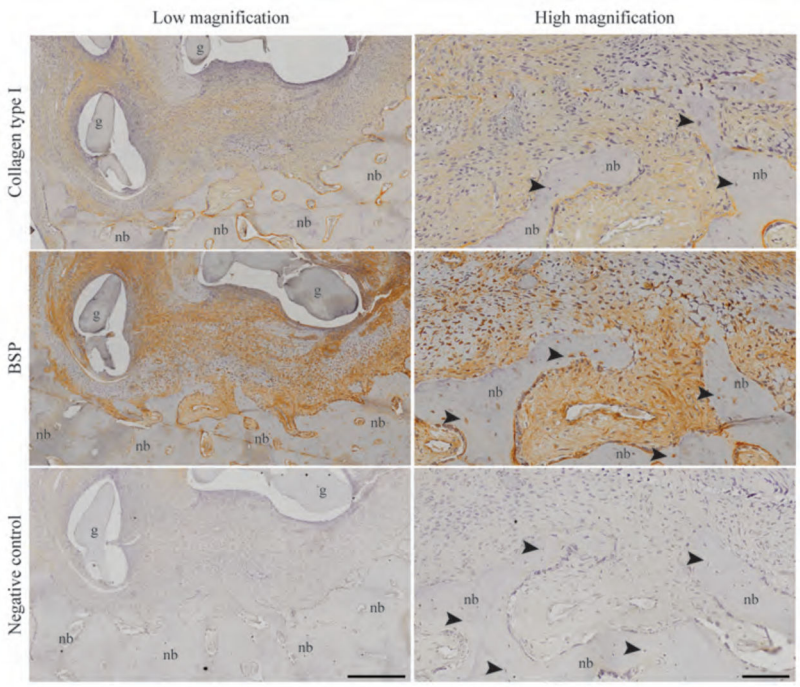

Figure 6. Deposition of type I collagen and bone sialoprotein (BSP) in the newly formed bone

The regenerating new bone (nb) within the tissue-engineered bone graft (g) is shown at low and high magnification. Localized areas of type I collagen and BSP at the graft-host bone interface were precursors for bone formation. New bone contained osteocytes (black arrowheads) within their lacunae. Negative immunohistochemistry confirmed the specificity of the staining. Images are representative of n=4 animals. Scale bars: 400 μm (low) and 100 μm (high).

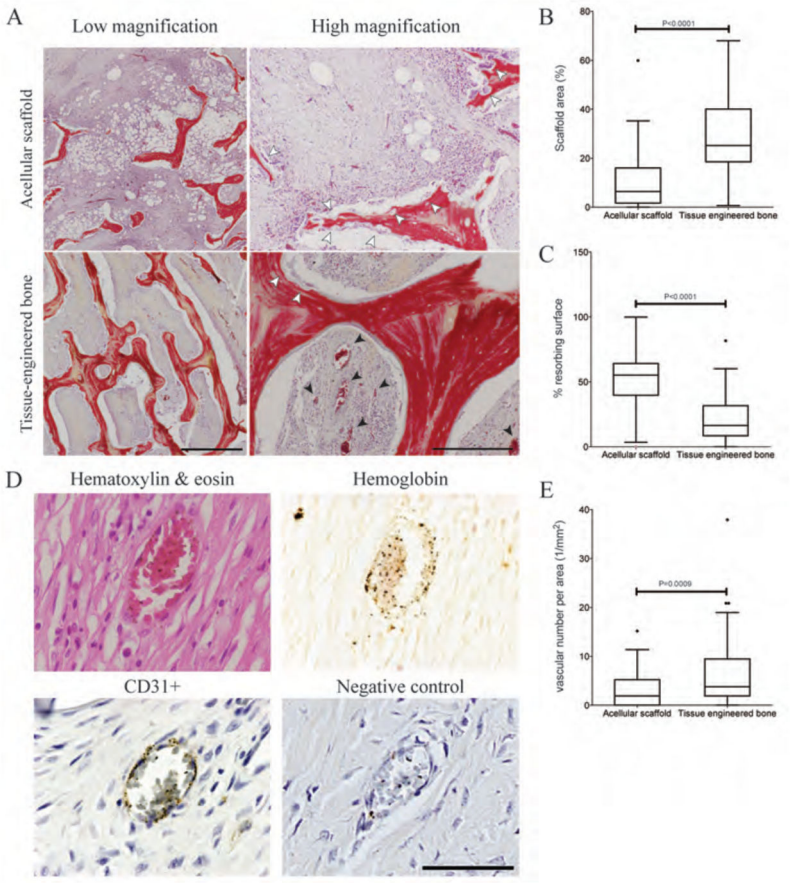

Figure 7. Graft resorption and vascularization

(A) Movat's pentachrome stain of the central region within the scaffolds is shown 3 months after implantation. Scaffold resorption is indicated by white arrows. Vasculature is indicated by black arrows. Scale bars: 1 mm and 250 μm. **(B, C)** Quantification of microstructure properties: percentage scaffold area (B), and percentage of the resorbing area (C). **(D)** H&E showed structural differences between the newly formed vasculature and the surrounding tissue. Immunohistochemistry for CD31 confirmed the presence of endothelial cell lining in newly formed vessels in both tissue engineered bone and acellular scaffold group. Negative control confirmed the specificity of CD31 antibody. The CD31 immunohistochmistry was used to quantify vascular number per area. Scale bar: 50 μm. **(E)** The number of blood vessels per area was quantified from CD31 immunohistochemical images. (B, C, E) Data are box plots for n = 56 images for the acellular scaffold group and n=90 images for the tissue-engineered bone group.